ISSN 1063-7737, Astronomy Letters, 2019, Vol. 45, No. 5, pp. 321–330. © Pleiades Publishing, Inc., 2019.
Russian Text © The Author(s), 2019, published in Pis'ma v Astronomicheskii Zhurnal, 2019, Vol. 45, No. 5, pp. 367–376.

A Water-Vapor Maser Flare in a High-Velocity Line toward W49N

L. N. Volvach[1*], A. E. Volvach[1,2], M. G. Larionov[3], G. C. MacLeod[4,5], P. Wolak[6], M. Olech[6], B. Kramer[7], K. Menten[7], A. Kraus[7], J. Brand[8,9], A. Zanicelli[8], S. Poppi[10], and S. Rigini[8]

[1]*Crimean Astrophysical Observatory, Russian Academy of Sciences, Nauchny, Crimea, 298409 Russia*

[2]*Institute of Applied Astronomy, Russian Academy of Sciences, nab. Kutuzova 10, St. Petersburg, 191187 Russia*

[3]*Astrospace Center, Lebedev Physical Institute, Russian Academy of Sciences, Profsoyuznaya ul. 84/32, Moscow, 117997 Russia*

[4]*Hartebeesthoek Radio Astronomy Observatory, P.O. Box 443, Krugersdorp 1740, South Africa*

[5]*University of Western Ontario, 1151 Richmond Street London, ON N6A 3K7, Canada*

[6]*Centre for Astronomy, Faculty of Physics, Astronomy and Informatics, Nicolaus Copernicus University, Grudziadzka 5, 87-100 Torun, Poland*

[7]*Max-Planck-Institut für Radioastronomie, Auf dem Hugel 69, D-53121 Bonn, Germany*

[8]*INAF - Istituto di Radioastronomia, Via Gobetti 101, I-40129 Bologna, Italy*

[9]*Italian ALMA Regional Centre, Istituto di Radioastronomia, Via Gobetti 101, I-40129 Bologna, Italy*

[10]*Osservatorio Astronomico di Cagliari, Via della Scienza 5, I-09047 Selargius (CA), Italy*

Received December 27, 2018; revised January 29, 2019; accepted January 29, 2019

Abstract—Powerful flares in Galactic kilomasers are closely associated with regions of intense star formation. They contribute to the elucidation of physical processes occurring in these structures. We have recorded a superpowerful flare in the high-velocity -81 km s^{-1} line in the Galactic maser source W49N. As a result of our monitoring at the RT-22 (Simeiz), RT-32 (Torun), RT-100 (Effelsberg), and RT-32 (Medicina) radio telescopes in the period from September 2017 to November 2018, we have obtained the shape of the spectral flux density variations in the source with time. At the peak the flux density reached $P \approx 5 \times 10^4$ Jy. The flare has a double pattern and different durations of its components. The pattern of spectral flux density variations for the first flare with a considerably shorter duration is apparently related to a sharp increase in the density of the medium and the photon flux and to a significant rise in the temperature to hundreds of kelvins. We propose a mechanism of primary energy release related to the existence of close massive multiple systems in star-forming regions. A powerful gravitational perturbation at the system's periastron can lead to a partial ejection of the envelope of the central massive star in a direction close to the major axis of the ellipse of the companion's orbit. This explains the significant asymmetry of high-velocity lines in W49N. The ejected envelope is an energy source more significant than the stellar wind and can explain the giant flares in the object. Further comprehensive studies in this direction, including monitoring VLBI studies, are needed to confirm this assumption.

DOI: 10.1134/S1063773719050074

Keywords: *star formation, radio lines, masers.*

INTRODUCTION

The maser source W49N is farther than the center of our Galaxy. It lies in a dense condensation located in a massive H_{II} region. The distance to the object is ∼15 kpc (Sato et al. 1967; Wynn-Williams 1971). According to more recent data, the object is closer, at a distance of ∼11 kpc (Zhang et al. 2013).

The bolometric luminosity of the infrared source associated with it is $L \sim 6 \times 10^5 L_0$, and as an exciting star (central source) it is necessary to have a massive star of early spectral type O5 (Heckman and Sullivan 1976).

This maser source is one of the richest by the set of water-vapor maser lines located in the velocity range ± 150 km s^{-1}. There are serious problems involved in explaining the line generation mechanisms in such a wide velocity range. In this case, it is necessary to follow the numerous observational facts accumulated since the discovery of masers.

Interferometric data suggest that both low-velocity

*E-mail: volvach@bk.ru

($\pm$15 km s^{-1}) and high-velocity ($>\pm$15 km s^{-1}) lines are initiated from a common center (Matveenko et al. 1988; Garay et al. 1989; Omodaka et al. 1999).

Moreover, there is evidence that the same maser spot (or very close spots) can provide the emission of several maser lines (Goldreich and Keeley 1972). Genzel et al. (1979) made an attempt to explain this emission of maser clumps. They considered the hyperfine structure of the water-vapor maser line (Zeeman and Stark effects), turbulence, and geometrical projection effects. Two more orders of magnitude were shown to be needed to explain the observational data (Morgan et al. 1978; Slysh 1973; Varshalovich et al. 2006).

Temperatures of 3×10^5 K, which, of course, are absent in maser emission regions, are required for the explanation by turbulence. Furthermore, it is difficult to imagine the generation of high-velocity lines without any symmetry relative to the local velocity system by turbulence.

A high degree of symmetry in a rotating gas–dust disk is required in the case of geometrical projection effects and the explanation may be considered only for low-velocity lines (Genzel et al. 1979).

The explanation of high-velocity maser features by supernova explosions was offered. The absence of nonthermal sources at the maser position was associated with the youth of supernovae (younger than 100 years) (Baudry et al. 1974). The authors themselves point out a low probability of this hypothesis, because the number of supernovae emerging in this case in the Galaxy is too large.

A kinematic source of high-velocity features with a positive shift, the Raman scattering model, is possible. Prohibitively high temperatures $T \approx 10^6$ K are required for its realization, which is totally unacceptable for the regions of maser clumps.

In this paper we present detailed observational data for one of the most powerful double flares of a water-vapor H_2O maser (the line frequency in the local standard of rest is 22.2350798 GHz) in the high-velocity -81 km s^{-1} feature. Possible emission mechanisms in high-velocity lines are considered.

THE OBSERVING TECHNIQUE AND DATA PROCESSING

The RT-22 radio telescope at the Crimean Astrophysical Observatory was equipped with a spectropolarimetric radiometer with a parallel Fourier spectrum analyzer to receive and record the signals from sources in the water-vapor line. The radiometer had 512 and/or 2048 channels. The radial velocity resolution was, respectively, 8 and 2 kHz in the H_2O line (Nesterov et al. 2000). The receiver bandwidth was 4 MHz when using the Mark-5B+ recording system and 16 MHz when recording the signal on the RDR1 recorder. The system noise temperature $T_{\rm noise}$ changed within the range 150–200 K, depending on the atmospheric conditions. The beam width of the radio telescope at 22 GHz (θ) was 150″. The atmospheric absorption was determined from the noise signal of a calibration step, from the so-called atmospheric cuts and fixed temperature differences at the RT-22 aperture $\Delta T_{\rm noise}$. The differences were made by loads at room and liquid nitrogen temperatures. The flux calibration was performed using the sources DR 21, Vir A, and Cyg A. The RT-22 sensitivity was 13 Jy/K.

The receiver for a wavelength of 1.35 cm was mounted at the RT-22 secondary focus. A highly stable frequency of 5 MHz from a VCH-1005 hydrogen frequency standard synchronized the frequency-tuned heterodynes. The input reception frequencies were converted to an intermediate frequency with the above bandwidths (Volvach et al. 2009). The observing cycle consisted of the signal accumulation for 5–10 min for on-source pointing and as much for an offset from the source by a fixed distance. The cycles could be repeated as many times as needed to achieve the desired signal-to-noise ratio. The data in linear polarization were received offline. The antenna temperature ($T_{\rm a}$) was calibrated using the calibration signal from a noise generators (NG). The NG temperature was established using the known temperature difference at the RT-22 aperture ($T_{\rm diff}$) that was provided by a matched load at the aperture.

The observing techniques at the Torun (Poland), Effeslberg (Germany), and Medicina (Italy) observatories were similar to those at RT-22 (Simeiz). At the Torun observatory the digital autocorrelator for 4096 channels had a velocity resolution of 26 m s^{-1}. The sensitivity of the radio telescope was 0.108 K/Jy.

When performing the observations with the Medicina 32-m radio telescope, the Xarcos system in one of the standard configurations (XK00) was used for recording, which allowed the observations in both left- and right-hand circular polarizations to be carried our simultaneously; furthermore, the zoom mode was additionally used (Melis et al. 2015). The spectra were obtained in four bands centered at the rest frequency of 22.235 GHz with a correction for the expected LSR velocity of the sources. The bands had a width of 62.5, 7.8, 2, and 0.5 MHz for 2048 channels, which gave a resolution of 30.5 kHz (0.44 km s^{-1}), 3.8 kHz (5.14×10^{-2} km s^{-1}), 0.95 kHz (1.29×10^{-2} km s^{-1}), and 0.24 kHz (3.21×10^{-3} km s^{-1}), respectively. The observations were carried out in the ON-OFF mode: 4 ON (on-source) cycles, 4 OFF (an offset from the source by 0.5° eastward)

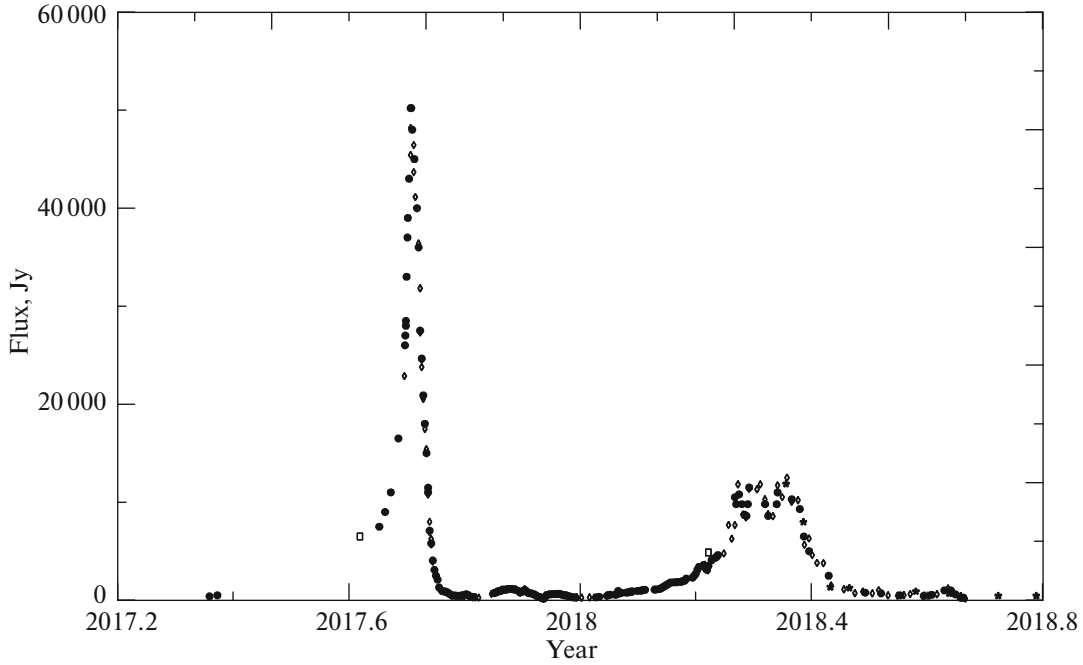

Fig. 1. Long-term monitoring of W49N in the water-vapor line at a velocity of −81 km s^{-1}: the filled circles, diamonds, squares, and asterisks indicate the Simeiz, Torun, Effelsberg, and Medicina data, respectively.

cycles, and 1 CAL (calibration) cycle, each with a duration of 30 s. The cycles were repeated three times for each source. The pointing accuracy was 5″–10″. The beam width at 22 GHz was ∼100″. The measured signals were corrected for atmospheric absorption. The variations in the effective area of the radio telescope with elevation and the antenna sensitivity were determined through the observations of the calibration sources 3C 48, 3C 123, 3C 286, and NGC 7027 using the flux densities from Perley and Butler (2013). The system temperatures at zenith (corrected for the atmosphere and elevation) were 120–150 K. The typical root-mean-square deviations were 0.7 Jy.

The observations at the Effeslberg 100-m telescope were carried out with a receiver for a wavelength of 1.3 cm mounted at the secondary focus. The central reception frequency was 22.235 GHz, the beam width was ∼38″. The spectral observations were performed using an FFT spectrometer with 65 535 channels. The bandpass was 100 MHz, the velocity resolution was about 20 m s^{-1}. The spectral data obtained in the observations were corrected for atmospheric absorption by taking into account the dependence of the telescope sensitivity on elevation. The conversion factor from the antenna temperature to the flux density was determined by the method of continuous observations (in the cross-scanning mode) of the calibration sources 3C 286, NGC 7027, etc. (Kraus et al. 2003).

MONITORING OF THE SPECTRAL FLUX DENSITY IN W49N IN THE HIGH-VELOCITY H_2O LINE

A long-term monitoring of W49N in the −81 km s^{-1} line was performed from September 2017 and during 2018. The data of spectral measurements were taken with a time interval of 1–2 days. Figure 1 shows the time dependence of the spectral flux density in the water-vapor lines at this velocity obtained from the line peaks.

It can be seen from Fig. 1 that the first, most powerful, flare is considerably shorter in duration than the second flare and a factor of 5 smaller in amplitude than the first one. One possible explanation of the second flare is that we can observe the successive line excitation in adjacent maser spots. The short-lived processes reflected in the shape of the first flare probably argue for a single maser spot initiated by a powerful shock physical phenomenon, which is most likely associated with the cataclysmic processes occurred in the central massive star of an early spectral type.

The presence of two types of flares occurred in close spatial regions may even be a typical case. We observed something similar in another most powerful Galactic kilomaser, G25.65+1.05 (IRAS 18316-0602) (Volvach et al. 2019a).

In Figs. 2 and 3 these flares are shown separately for more convenient perception of their shape and details. Any new information about the pattern of spectral flux density variations in the water-vapor maser

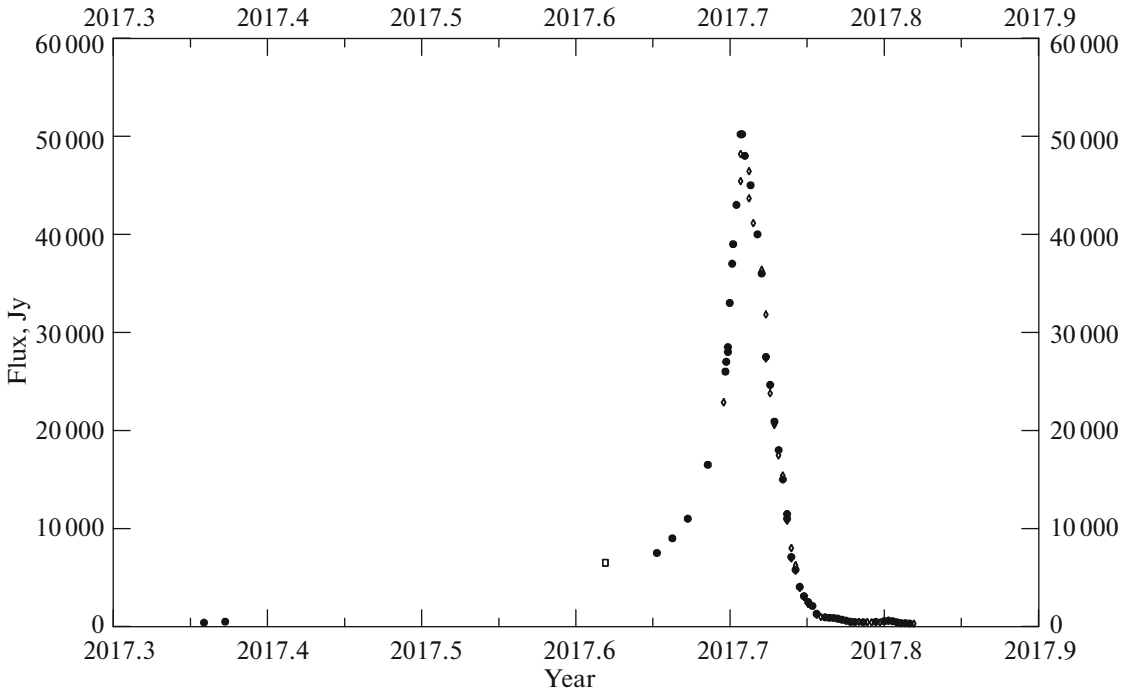

Fig. 2. Long-term monitoring of W49N in the water-vapor line at a velocity of -81 km s^{-1} for the first flare: the filled circles, diamonds, and squares indicate the Simeiz, Torun, and Effelsberg data, respectively.

line and variations in its spectral characteristics is of great importance for studying the line pumping mechanism and the dynamics of maser regions.

An analysis of the flux density monitoring curve during a high-velocity flare leads to fundamental conclusions.

The shapes of both first and second flares are asymmetric (Figs. 2 and 3). The leading edges can be fitted by an exponential dependence. The exponential shape of the maser flux density curve serves as a very important sign of the maser state during a flare: it operates in an unsaturated regime, when the maser amplification increases exponentially with pumping rate (Goldreich et al. 1973).

In Fig. 4 the inverse of the square of the line width is plotted against the flux for the first (upper plot) and second (lower plot) flares. Both dependences run almost parallel to each other, but they differ by the line width. The difference is that at the maximum phases the line width is ~50 and ~65 kHz in the first and second flares, respectively.

The linear flux dependence of the square of the line width in the minus first power suggests that the maser is in an unsaturated regime. Similar results were also obtained for the giant flares in Orion KL and IRAS 18316-0602 (Omodaka et al. 1999; Shimoikura et al. 2005; Volvach et al. 2019a). In all cases, it was concluded that the masers are in an unsaturated state up to the maximum flare amplitude.

The width (~50 kHz) and shape of the high-velocity maser line in W49N near the maximum phase of the first flare provide evidence for the fact that we observe the emission from the single-component source responsible for the bulk of the increase in flux density (Fig. 5a). The width (~65 kHz) and shape (slightly asymmetric) of the high-velocity maser line in W49N near the maximum phase of the second flare suggest that several maser spots with slightly different physical characteristics were involved in the formation of the second flare (Fig. 5b).

The frequencies of the first and second flares coincide, which may point to the spatial proximity of the clumps emitting them or to the fact that the emission of the first and second flares comes from the same maser spot. In the latter case, it is required to explain why the characteristics of the clump in the second flare changed, the line width increased.

If the first and second flares are assumed to have occurred in different maser spots, then we can estimate the maximum distance between the emitting spots based on the delay time between the flares and the possible velocity of the maser spot excitation component. The time between the flares is about half a year, $\Delta T \approx 3 \times 10^7$ s. The velocity of the ejected envelope of the central star or the shock front is $v \approx 200$ km s$^{-1} = 2 \times 10^7$ cm. The distance between the maser spots is then $\Delta r \approx 6 \times 10^{14}$ cm ≈ 40 AU.

A broadband spectrum of maser lines is presented in Fig. 6. The -81 km s^{-1} line under study was

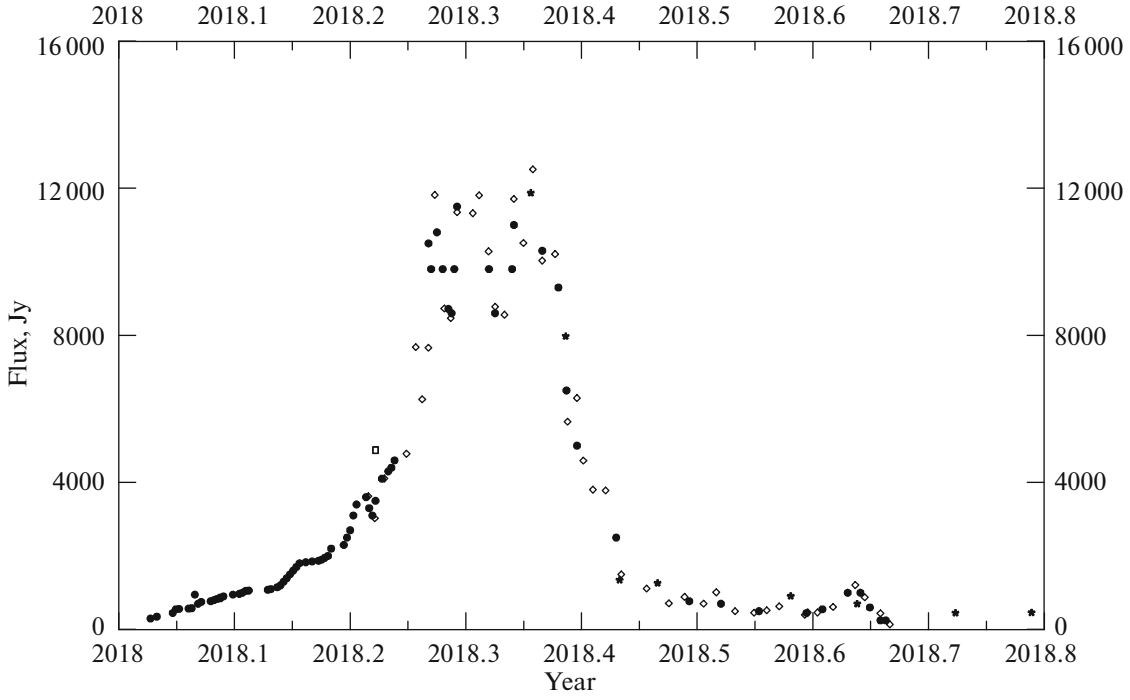

Fig. 3. Long-term monitoring of W49N in the water-vapor line at a velocity of -81 km s^{-1} for the second flare: the circles, diamonds, squares, and asterisks indicate the Simeiz, Torun, Effelsberg, and Medicina data, respectively.

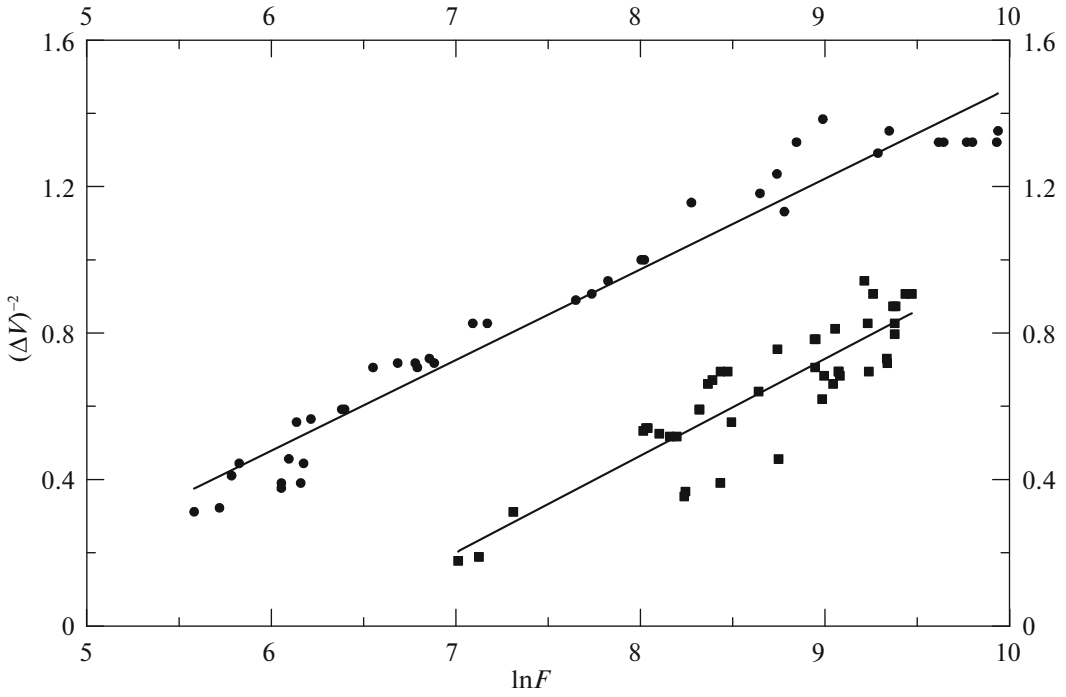

Fig. 4. Inverse of the square of the line width Δv^{-2} (km s^{-1}) versus natural logarithm of the flux lnF (Jy). The upper and lower inclined dependences are for the first and second flares, respectively.

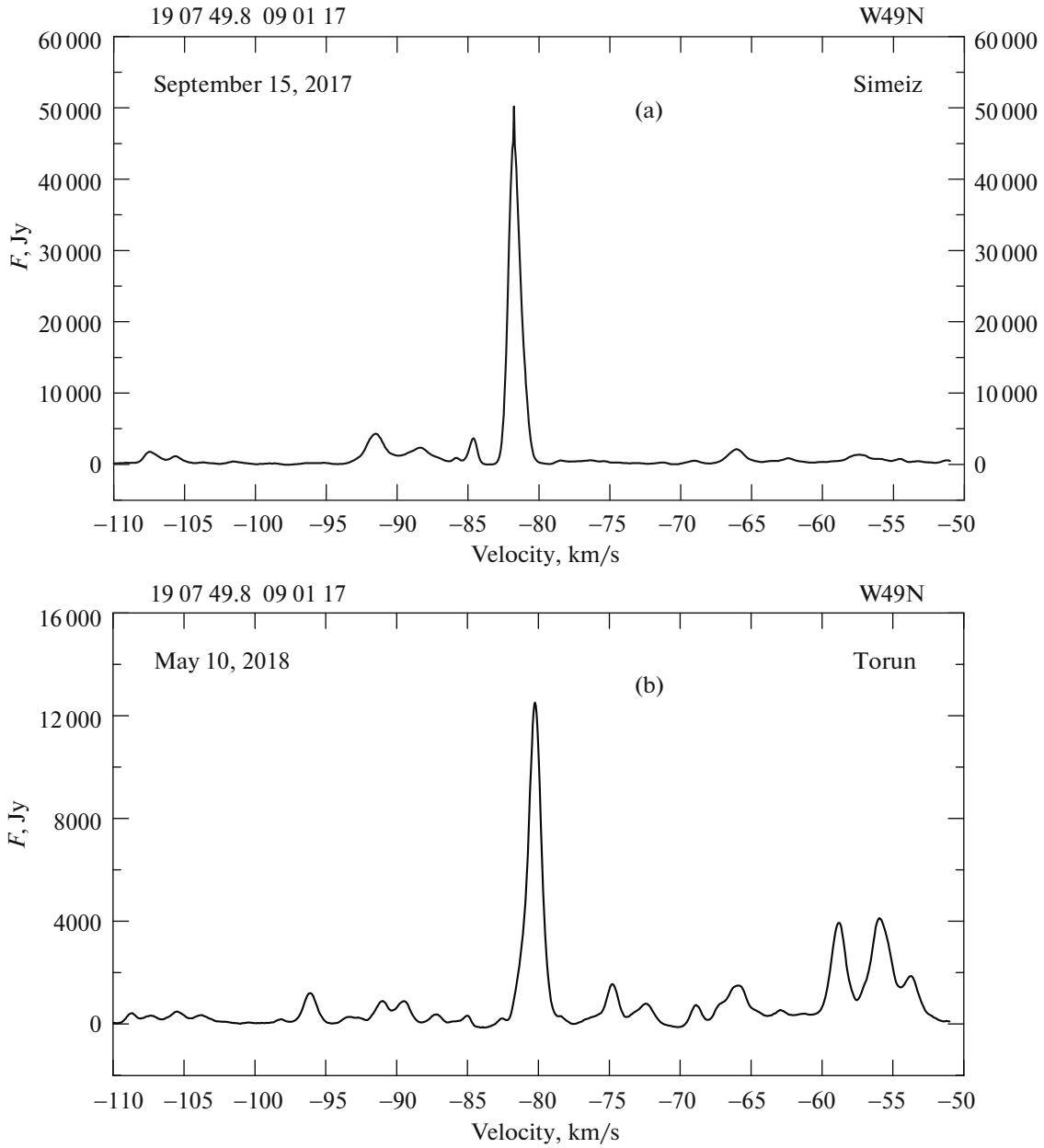

Fig. 5. (a) The -81 km s^{-1} at the peak of the first high-velocity flare. (b) The line at the peak of the second high-velocity flare.

not particularly pronounced against the background of other adjacent lines half a month before the flare onset. Nevertheless, the richness of high-velocity lines in the negative spectral range is obvious. The asymmetry is present and, in principle, requires a physical justification.

DISCUSSION

The high-velocity lines in W49N are distributed in the velocity range ± 150 km s^{-1} and account for less than 10% of the low-velocity lines energy (Heckman and Sullivan 1976). They are concentrated to a greater extent in the negative spectral range. It was established by interferometric observations that the emission region in these lines is more compact than that in the low-velocity ones. It is less than 10^4 AU in size and lies on the periphery of the low-velocity lines (Knowles et al. 1974).

It has long been noticed that the lines are variable on time scales of several months. There was a correlation of the line flux densities over the entire spectrum for both high-velocity and low-velocity lines (Sullivan 1973). It was suspected that the positions of individual emission regions, whose sizes were no less

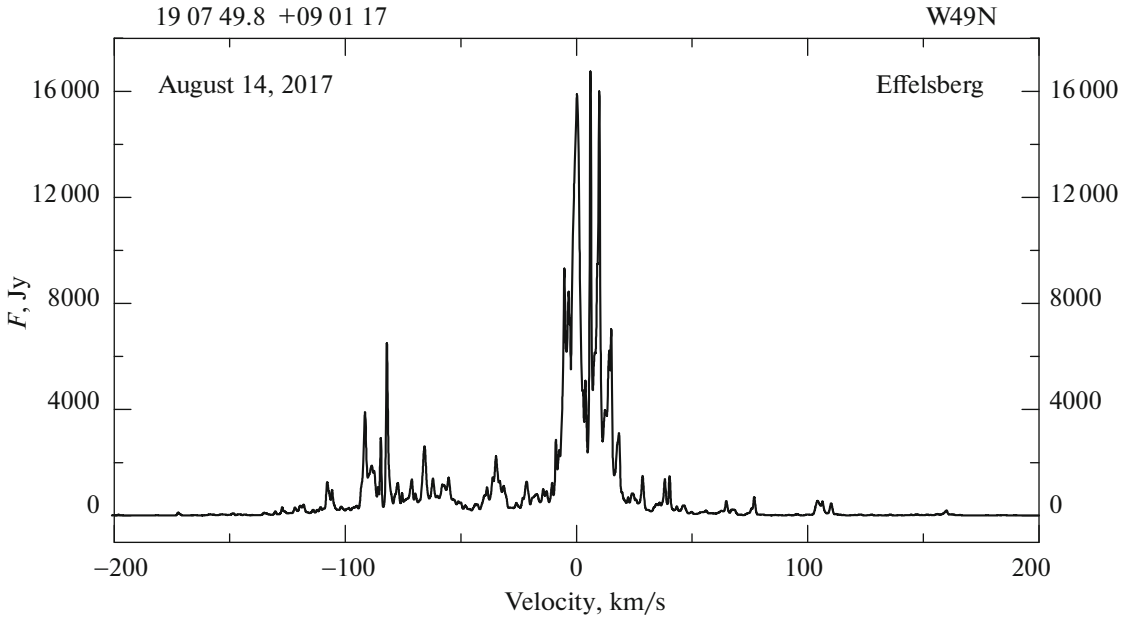

Fig. 6. Broadband spectrum of water-vapor maser lines in W49N.

than those for the low-velocity lines, changed with time (Knowles et al. 1974).

An important fact is that the high-velocity lines in W49N have lower intensities and frequency shifts relative to the low-velocity ones (Goss et al. 1976). The narrow range of line widths is not confirmed by our data (Fig. 4). The ranges of high-velocity line widths are no less than those for the low-velocity ones.

The high-velocity lines in W49N and, in particular, the line under study have velocities that exceed the isothermal sound speed, which is within 10 km s^{-1}, by tens of times or more. On the other hand, Larson (1973) showed that the accretion of material onto a protostar has a limitation in velocity of only a few sound speeds and, therefore, cannot explain the appearance of high-velocity lines in W49N.

If, however, the objects containing maser sources with high-velocity lines move themselves with such velocities, then they are dynamically unstable objects in the case of W49N (Strel'nitskii and Sunyaev 1972). The latter stems from the fact that the high-velocity masers are concentrated in a region with a size of only 0.1 pc. The above authors proposed three possible acceleration mechanisms that give rise to high-velocity lines in water-vapor masers: the acceleration through radiation pressure, by the the stellar wind from hot massive stars, and by the shock waves propagating in the space occupied by masers. Silk added one more admissible acceleration mechanism, the shock waves from supernova explosions (Silk and Burke 1974). For example, W49B is known to be a supernova remnant. However, the fact that there is no nonthermal source, which is a signature of a supernova remnant, at the position of W49N is disturbing. Nevertheless, young supernovae with an age up to 100 years are known to give no noticeable radio emission and, therefore, are not detected (Spencer and Burke 1973).

An additional condition for the presence of a noticeable radio emission is the necessity of sweeping up a large amount of interstellar material comparable to the mass of the exploded supernova remnant (Gull 1973). Otherwise, a detectable emission emerges only in the period of the supernova explosion itself.

The size and age of the supernova remnant depends on the mass and energy of the expanding envelope. For example, an envelope of one solar mass with a kinetic energy of 10^{51} erg expanding into a surrounding space with a density of one hydrogen atom per cm^{-3} reaches an age of 80 years, having a diameter of 1.6 pc (Baudry et al. 1974). In this case, at the distance of W49N we will see a nonthermal nebula with a size of 11″.

The actual density in the region of maser objects W49N must be much higher and, therefore, for a density of 10^3 cm^{-3} the epoch of emergence of a noticeable radio emission is reduced by an order of magnitude, along with the angular sizes (Baudry et al. 1974). Higher-resolution observations of nonthermal nebulae are already required in this case.

When talking about possible models for the generation of emission in high-velocity lines, the scheme proposed in other papers should be mentioned. For example, the model of a low-mass protostar in a

T Tau-like phase of evolution accompanied by a stellar mass loss was considered (Strom et al. 1974). Optical lines with velocities of -100 km s^{-1} were found in Herbig–Haro objects (Kuhi 1964). Nevertheless, such models run into the difficulties involved in interpreting the observational data (Heckman and Sullivan 1976).

For high-velocity lines there is an additional problem of explaining the asymmetry of the positive and negative emission regions in lines. The models of a uniform spherical expansion of the gas clouds around the central star are commonly used (Herbig 1974). The introduction of emission beaming is controversial. Besides, we know the cases where detailed observational data were obtained, as in our case, suggesting an asymmetric shape of the time dependence of the spectral flux density in a line, that rule out the emission beaming effects (Fig. 1). The theories of beamed emission predict the existence of masers in an unsaturated state, for example, as in the case of the Galactic kilomaser G25.65+1.05 (IRAS 18316-0602) (Volvach et al. 2019a).

There is an assumption that the presence or absence of positive or negative high-velocity maser lines is a chance coincidence in the distribution of masses around the central massive star. The studies by Goss et al. (1975) confirmed this assumption.

Another class of "asymmetric" models is associated with the scattering of photons (Radhakrishnan et al. 1975). The homogeneous scattering models do not pass for energy reasons. Furthermore, the Raman scattering models do not allow the spectral and spatial dependences obtained from observational data to be explained (Boyd 1977).

The change of the high-velocity lines in W49N recorded in 1974–1976 revealed two significant flares occurred at -41 and -83 km s^{-1}. The amplitudes of these two flares did not exceed 25 kJy. The peaks of the first and second flares occurred in 1976 and 1974, respectively (Little et al. 1977). In 1975 the -83 km s^{-1} flare had an amplitude of less than 500 Jy. A careful analysis of Fig. 3 from Little et al. (1977) shows that the -83 km s^{-1} flare at a certain stage of development (at the maximum phase) reveals a second component with an amplitude of about 5 kJy located precisely at -81 km s^{-1}. The resolution of the spectrometer used (0.8 km s^{-1}) allowed the second component to be identified quite clearly. Moreover, the flare in 1974 was close in frequency position to ours, given that the difference is only two standard deviations, and a frequency drift is possible even within one flare.

This example shows that individual features can retain their frequency positions for more than 40 years. This, in turn, is some record of the duration water-vapor maser lines if the fact that this is a high-velocity line is additionally taken into account.

When interpreting the mechanisms for the formation of high-velocity maser lines, we should take into account the fact of temporal stability, along with the existence of a significant spectral asymmetry toward negative values. The model of pulsationally unstable massive stars was proposed (Parfenov and Sobolev 2014). In this case, the authors attempted to explain the presumed cyclicity of flares by the colliding stellar winds of binary stars (Inayoshi et al. 2013).

The principle of the approach itself, which is related to the binarity of massive stars, seems quite productive. Therefore, previously (Volvach et al. 2019b) we came up with the idea of the initiation of primary energy release in massive multiple stars of an early spectral type. The primary energy release can be associated with the partial ejections of a part of the envelope of the central star under the action of a sufficiently massive companion at the periastron of a multiple star system.

It is not inconceivable that a known fraction of massive stars at an early evolutionary stage are binary or multiple systems formed during the evolution of a gas–dust cloud. Close massive systems can be formed during the evolution and a powerful gravitational interaction emerges between them. In this case, it becomes possible to initiate the sources of primary energy release in gas–dust clouds through the partial ejection of the envelope of the central massive star due to the gravitational interaction from the companion at the system's periastron. From the energy standpoint, such ejections of the envelope can provide the energetics of the maser emission process and explain the giant flares that occasionally occur, for example, once in 10–20 years.

Such ejections can be asymmetric and the preferential direction of the ejection depends on the orientation of the orbit. This can explain the fact that in different maser systems we see a predominance of high-velocity lines of a particular sign.

The expenditure of energy needed for the formation of a maser line can be estimated. The flux on the Earth's surface is $F_{\rm E} \approx 5 \times 10^4$ Jy. Given the distance from the Earth to W49N ($\sim$11 kpc) and the maser line emission bandwidth ($\sim$50 kHz), we obtain a line luminosity $L_g \approx 0.1 L_0$. The ratio of the luminosity of the central star $L_\star \approx 6 \times 10^5 L_0$ to the line luminosity is $N \approx 6 \times 10^6$. The scattering factor of the energy going from the star to the maser clump should be additionally taken into account. An energy fraction $N_g \approx (R_g/R_n)^2 \approx (10^{13}/10^{15})^2 \approx 10^{-4}$, where R_g are the maser spot size and R_n is the distance from the star to the clump, reaches it. The

necessary expenditure of energy to provide the maser emission is then $L \approx L_g/N_g \approx 10^3 L_0$ and the ratio $L/L_\star \approx 1.7 \times 10^{-2}$. In this case, about 2% of the luminosity of the central star spent during the flare action is required for the emergence of a giant flare in W49N.

The ejected envelope must have an energy of at least $E \approx L \times T = 10^5 L_0 \times 1.5 \times 10^7 \approx 1.5 \times 10^{45}$ erg, where T is the flare duration. For example, in the time of its evolution ($\sim 10^6$ yr) a massive star can give up $E_\star \approx 10^{-2} M_\star c^2 \approx 1.2 \times 10^{54}$ erg into the surrounding space, i.e., a billion times more.

Given that the velocity of the ejected envelope $v \approx 10^7$ cm s^{-1}, the mass of the ejected envelope is $M \approx E/v^2 \approx 1.5 \times 10^{31}$ g $\approx 1.5 \times 10^{-4} M_\star$.

Hence it can be concluded that many partial ejections of the envelope of the central massive star can occur in its evolution time.

For W49N the maser superflares under consideration lasted about one year. Given the presence of a high-velocity feature near 100 km s^{-1} in the source, we have a velocity of the ejected envelope $v \approx 10^7$ cm s^{-1} (100 km s^{-1}) and the distance to which the envelope will move in the maser clump activation time (6 months), $l \approx 1.5 \times 10^{14}$ cm (about 11 AU), which exceeds the sizes of maser structures by more than an order of magnitude. In order that the maser be in an activated state, it is necessary to have an ejected envelope extending over 11 AU. Based on the fact that the stars can also be at pericenter for a longer time (Volvach et al. 2019b), this maser emission activation mechanism is quite possible.

Based on the characteristic time between flares, we can estimate approximate orbital parameters of the system's companion in W49N. In the time of long-term observations of the source since its discovery, single powerful water-vapor maser flares were recorded in the object. Using a characteristic time between flares of 10 years, based on the laws of celestial mechanics, we will obtain the size of the elliptical orbit with a semimajor axis of $\sim$30 AU for a massive central star of mass 50 M_0 in a pair with a less massive object. Thus, being at the system's pericenter, the companion of the massive central star pulls off and ejects some stellar mass moving with a velocity of several hundred km s^{-1} and operating as a very powerful stellar wind into the surrounding space.

A further monitoring of the object with single antennas and VLBI studies in the dynamic regime are needed to confirm the proposed concept.

CONCLUSIONS

(1) We performed a long-term monitoring of the Galactic kilomaser W49N in the high-velocity water-vapor line using the RT-22 (Simeiz), RT-32 (Torun), RT-100 (Effelsberg), and RT-32 (Medicina) radio telescopes.

(2) We recorded a detailed shape of the flux density curve during the unique giant double flare that lasted from September 2017 and during 2018.

(3) We obtained evidence that during the flare the kilomaser operated in an unsaturated regime: an exponential rise and a peculiar flux dependence of the line width were observed.

(4) The curves of flux variations with time in giant flares in different sources, W49N, Orion KL, and IRAS 18316-0602, were found to coincide in shape, which can confirm the thesis that the processes occurring during water-vapor maser flares are identical.

(5) The line shapes in the two our flares are not identical and may suggest that the flares occurred in different sources.

(6) We considered possible stimulators of energy release in the system that lead to giant flares of kilomasers and increase their flux by tens of times.

ACKNOWLEDGMENTS

We thank the National Science Center of Poland, grant no. 2016/21/B/ ST9/01455.

FUNDING

This work was supported in part by Russian Science Foundation grant no. 19-12-00074 and Program 12 of the Russian Academy of Sciences. The work is based in part on the observations at the Effelsberg 100-m telescope of the Max-Planck-Institut für Radioastronomie.

REFERENCES

1. A. Baudry, J. R. Foster, and W. J. Welch, Astron. Astrophys. **36**, 217 (1974).
2. R. W. Boyd, Pabl. Astr. Soc. Pacif. **89**, 141 (1977).
3. G. Garay, J. M. Moran, and Haschick, Astron. J. **338**, 244 (1989).
4. R. Genzel, D. Dowens, J. M. Moran, K. J. Johnston, J. H. Spencer, L. I. Matveenko, L. R. Kogan, V. I. Kostenko, et al., Astron. Astrophys. **78**, 239 (1979).
5. P. Goldreich and D. A. Keeley, Astron. J. **174**, 517 (1972).
6. P. Goldreich, D. A. Keeley, and J. J. Kwan, Astrophys. J. **179**, 111 (1973).
7. W. M. Goss, S. H. Knowles, M. Balister, R. A. Batchelor, and K. J. Wellington, Mon. Not. R. Astron. Soc. **174**, 541 (1976).

8. S. F. Gull, Mon. Not. R. Astron. Soc. **161**, 47 (1973).
9. T. M. Heckman and W. T. Sullivan, Astrophys. J. **17**, 105 (1976).
10. G. H. Herbig, Astrophys. J. **189**, 75 (1974).
11. K. Inayoshi, K. Sugiyama, and T. Hosokawa, Astrophys. J. **773**, 70 (2013).
12. K. J. Knowles, J. M. Johnston, B. F. Morgan, et al., Astron. J. **79**, 925 (1974).
13. A. Kraus, T. P. Krichbaum, R. Wegner, et al., Astron. Astrophys. **401**, 161 (2003).
14. L. V. Kuhi, Astrophys. J. **140**, 1409 (1964).
15. R. B. Larson, Ann. Rev. Astron. Astrophys. **11**, 219 (1973).
16. L. T. Little, G. J. White, and P. W. Riley, Mon. Not. R. Astron. Soc. **180**, 639 (1977).
17. L. I. Matveenko, D. A. Graham, and P. J. Diamond, Sov. Astron. Lett. **14**, 468 (1988).
18. A. Melis, C. Migoni, G. Comoretto, et al., SRT Int. Rep. **52** (2015).
19. J. M. Morgan, M. J. Reid, C. J. Lada, et al., Astron. J. **224**, L67 (1978).
20. N. S. Nesterov, Vol'A. E. vach, I. D. Strepka, et al., Radiofiz. Radioastron. **5**, 320 (2000).
21. T. Omodaka, T. Maeda, M. Miyoshi, et al., Publ. Astron. Soc. Jpn. **51**, 333 (1999).
22. S. Yu. Parfenov and A. M. Sobolev, Mon. Not. R. Astron. Soc. **444**, 620, 30 (2014).
23. R. A. Perley and B. J. Butler, Astrophys. J. Suppl. Ser. **204**, 19 (2013).
24. V. Radhakrishnan, W. M. Goss, and R. Bhandari, Pramana **5**, 51 (1975).
25. F. Sato, F. Akabane, and F. J. Kerr, Austral. J. Phys. **20**, 197 (1967).
26. T. Shimoikura, H. Kobayashi, T. Omodaka, et al., Astrophys. J. **634**, 459 (2005).
27. J. Silk and J. R. Burke, Astrophys. J. **190**, 11 (1974).
28. V. I. Slysh, Astrophys. J. **14**, 213 (1973).
29. J. H. Spencer and B. F. Burke, Astrophys. J. **185**, L83 (1973).
30. S. E. Strom, G. L. Grasdalen, and K. M. Strom, Astrophys. J. **191**, 111 (1974).
31. W. T. Sullivan, Astrophys. J. Suppl. Ser. **25**, 393 (1973).
32. V. S. Strel'nitskii and R. A. Sunynyaev, Sov. Astron. **16**, 579 (1972).
33. D. A. Varshalovich, A. V. Ivanchik, and N. S. Babkovskaya, Astron. Lett. **32**, 29 (2006).
34. A. E. Volvach, L. N. Volvach, I. D. Strepka, et al., Izv. Krymsk. Astrofiz. Observ. **104**, 72 (2009).
35. L. N. Volvach, A. E. Volvach, M. G. Larionov, G. C. MacLeod, S. P. van den Heever, P. Wolak, and M. Olech, Mon. Not. R. Astron. Soc. **482**, L90 (2019a).
36. L. N. Volvach, A. E. Volvach, M. G. Larionov, et al., Astron. Rep. **63**, 49 (2019b).
37. C. G. Wynn-Williams, Mon. Not. R. Astron. Soc. **151**, 397 (1971).
38. B. Zhang, M. J. Read, R. M. Menten, et al., Astrophys. J. **79**, 13 (2013).

Translated by V. Astakhov